TiO$_2$-photocatalyzed transformation of the recalcitrant X-ray contrast agent diatrizoate

Matthew N. Sugihara, Diane Moeller, Tias Paul, Timothy J. Strathmann*

Department of Civil and Environmental Engineering and Center of Advanced Materials for the Purification of Water with Systems, University of Illinois at Urbana-Champaign, Newmark Civil Engineering Laboratory, MC-250, Urbana, IL 61801, USA

ARTICLE INFO

ABSTRACT

Iodinated X-ray contrast media (ICM) are biologically recalcitrant chemicals that are often detected in wastewater-impacted environments at higher concentrations than other pharmaceutical micropollutants of concern. Diatrizoate is an anionic ICM that is especially resistant to conventional wastewater and drinking water treatment processes. This study examined the aqueous photocatalytic treatment of diatrizoate using nanophase titanium dioxide (TiO$_2$). Experiments demonstrated that diatrizoate can be degraded in aqueous TiO$_2$ suspensions illuminated with ultraviolet-A (UVA) light. In oxic solutions, diatrizoate degraded principally via oxidation by adsorbed hydroxyl radicals (•OH), releasing iodine substituents stoichiometrically, but causing little mineralization of organic carbon and nitrogen. Introduction of •OH scavengers significantly slowed the rate of photocatalytic degradation. At circumneutral pH, diatrizoate was oxidized much more slowly than iopromide, a nonionic ICM, in part because of unfavorable electrostatic interactions with the negatively charged TiO$_2$ surface; increased rates of oxidation observed at lower pH conditions can be attributed to more favorable diatrizoate-TiO$_2$ sorptive interactions. Experiments also demonstrated that diatrizoate was degraded at appreciable rates in anoxic solutions, and reductive dehalogenation products are identified by liquid chromatography–mass spectrometry. The higher selectivity of reductive processes suggests a promising strategy for targeted treatment of recalcitrant ICM in organic-rich matrices like wastewater effluent.

© 2012 Elsevier B.V. All rights reserved.

1. Introduction

A growing body of research has documented widespread occurrence of pharmaceuticals and personal care products (PPCPs) in wastewater effluent-impacted waters, raising serious concerns about affected aquatic ecosystems and public health [1–5]. Although measured concentrations of individual PPCPs are typically very low (ng L^{-1} to μg L^{-1}), little is known about chronic exposure to sub-therapeutic levels of PPCPs over many years or the potential for additive and synergistic toxicological effects when exposed to mixtures of PPCPs [1,2]. Many PPCPs have been found to be recalcitrant to conventional drinking water and wastewater treatment processes [2,4,5], so there is considerable interest in the development of more effective and sustainable technologies for treating water contaminated with many different PPCPs [6–10].

Iodinated X-ray contrast media (ICM) (Table 1), a class of medical diagnostic agents used for imaging blood vessels and organs, are among the most recalcitrant and highly persistent PPCPs [11–14]. Large quantities of ICM are administered to individual patients undergoing tests (>100 g dose^{-1}), and they are resistant to human metabolism by design and are generally excreted unmetabolized within 24 h [15]. Worldwide use of ICM has been reported to be on the order of 3.5×10^6 kg yr^{-1} [16]. Due to their heavy use and high biochemical stability, elevated concentrations of ICM have been detected in hospital and domestic wastewater, treated wastewater effluent, surface water, groundwater, and even finished drinking water [12,13,17–19]. Although often considered to be biochemically inert, some research has shown that diatrizoate may have nephrotoxic effects in animals and humans [20,21].

Only limited biodegradation of ICM has been reported during biological wastewater treatment processes and biotransformation is very slow in soil/sediment–water incubations (e.g., $t_{1/2} > 20$ days) [13,22,23], resulting only in partial modifications to the side chains of the core triiodinated aromatic ring structure [22,23]. Conventional drinking water treatment processes have also been found to have little success in removing or transforming ICM [24]. Advanced treatment processes like ozonation have shown some success in degrading ICM, attributed to reactions with hydroxyl radicals (•OH), powerful non-selective oxidants that form during O$_3$ decomposition [9,25], and better ICM removal occurs during treatment with ozone-based advanced oxidation processes (AOPs) that promote •OH formation (e.g., UV/O$_3$, O$_3$/H$_2$O$_2$) than during O$_3$

Table 1
Structures of ICM and structural analogues examined.

diatrizoate (DIA)   iopromide (IOP)   3,5-diacetamidobenzoate (DABA)
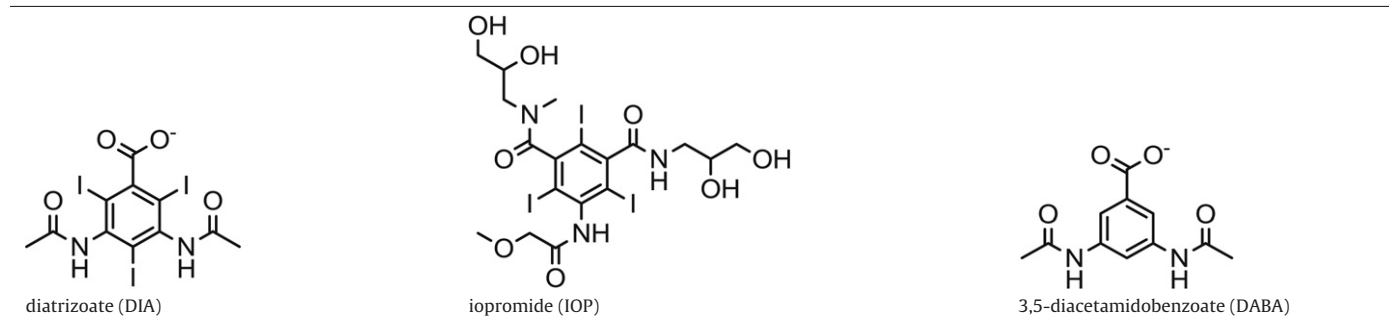
treatment processes where $^\bullet$OH production is not specifically promoted [25]. Recent work also shows that reductive dehalogenation of the central ring structure can be mediated by treatment with zerovalent iron or H_2 in combination with metal catalysts (Pd, Ni) [26–28].

Photocatalytic treatment processes using semiconductors like titanium dioxide (TiO_2) have emerged as a promising nanotechnology for treating waters contaminated with highly recalcitrant organic contaminants. TiO_2 nanomaterials are generally considered to be the most practical semiconductor photocatalysts for water treatment applications because of their low cost, small bandgap energy, high chemical stability, and low water solubility [29]. Ultraviolet (UV) light with energy exceeding the semiconductor bandgap energy of TiO_2 ($E_{bg} = 3.2$ eV for anatase, corresponding $\lambda < 385$ nm [30]) excites electrons from the filled valence band to an empty conduction band, leading to charge separation and formation of strongly oxidizing valence band holes (h_{vb}^+) and strongly reducing conduction band electrons (e_{cb}^-). These species can migrate to the catalyst surface, where h_{vb}^+ oxidizes adsorbed H_2O/OH^- to form $^\bullet$OH, a strong non-selective oxidant that reacts with most organic chemicals at near diffusion-limited rates [31–33]. Conversely, the photo-generated e_{cb}^- can react with an adsorbed electron acceptor, typically O_2 in oxic waters [29]. Conduction band electrons in TiO_2 have a very low reduction potential (-0.84 V at pH 7) [34] and are also capable of reducing contaminants with oxidized structures, including nitroaromatic explosives and halogenated solvents [34–37]. In complex organic-rich matrices (e.g., wastewater effluent), additional reactions need to be considered, including reactions of secondary oxidant and reductant species produced when non-target water constituents (e.g., natural organic matter) react with primary reactive species generated by excitation of the photocatalyst.

Little work exists on the photocatalytic treatment of ICM, especially ionic ICM like diatrizoate that have been shown to be remarkably resistant to biotransformation [23,38,39]. Doll and Frimmel [40–42] reported on the UV-TiO_2 photocatalytic degradation of nonionic ICM (iomeprol and iopromide), demonstrating significant rates of degradation and liberation of iodine substituents from the central ring structure, but only limited mineralization of organic carbon. Although these studies report degradation kinetics for ICM by UV-TiO_2, experiments designed to identify the photo-generated reacting species and the controlling reaction mechanisms and pathways were not reported. In addition, past work was limited to photocatalytic transformation processes occurring in oxic solutions, and the potential for TiO_2-reductive photocatalytic transformation in anoxic solutions have not been reported. Such processes may be especially useful for transforming the highly recalcitrant central triiodinated ring structure in ICM to more biodegradable products.

This contribution examines the kinetics and mechanisms for TiO_2 photocatalytic transformation of diatrizoate and structurally

related compounds (Table 1) in both oxic and anoxic aqueous suspensions. Experimental work was conducted to (i) quantify the effects of solution conditions on rates of diatrizoate photocatalytic degradation, (ii) assess the influence of diatrizoate structure on reaction rates, (iii) identify the photo-generated reactive species responsible for diatrizoate transformation, (iv) quantify the extent of mineralization and identify selected organic transformation products, and (v) characterize pathways responsible for photocatalytic transformation of diatrizoate under both oxic and anoxic conditions. Results from this study provide new insights into the mechanisms and environmental factors controlling photocatalytic transformation of ICM, and support the further development of practical photocatalytic treatment technologies for waters contaminated with ICM and other classes of recalcitrant organic micropollutants.

2. Experimental

2.1. Materials and reagents

All reagents were of high purity and were used as received from suppliers. Diatrizoate (DIA: 2,4,6-triiodo-3,5-diacetamidobenzoate, sodium salt) and its deiodinated analogue (DABA: 3,5-diacetamidobenzoic acid), NaOH, $NaClO_4$, NaI, $NaNO_3$, $NaNO_2$, NH_4Cl, $NaHCO_3$, triethylamine, NaH_2PO_4, Na_2HPO_4, $HClO_4$, and ammonium acetate were purchased from Sigma-Aldrich-Fluka (St. Louis, MO). Iopromide (IOP) was provided as a gift from Schering AG (Berlin, Germany). Methanol, acetonitrile, and H_3PO_4 were obtained from Fisher Scientific (Fairlawn, NJ). Ultra-zero grade air and argon gases were obtained from S.J. Smith Welding Supply (Urbana, IL). Total organic carbon reference standards were obtained from VWR (West Chester, PA). All aqueous solutions were prepared using laboratory-grade deionized water (>17.3 MΩ cm; Barnstead Nanopure system).

Photocatalysis experiments were conducted using a nanophase TiO_2 (Type P25) supplied by Degussa (Düsseldorf, Germany). Degussa P25 TiO_2 has been extensively used as a model photocatalyst [7,10,35–37,40–43] and is a mixed nanophase material containing approximately 70% anatase and 30% rutile with a specific surface area of 55 $m^2 g^{-1}$ [29]. Aqueous stock suspensions of TiO_2 were prepared >24 h prior to use to ensure hydration of the catalyst particle surfaces.

2.2. Light source

Reactors were illuminated using an Oriel O_3-free 450 W xenon arc lamp system (Oriel, Model 66921). Collimated light was first passed through a 10 cm water filter to remove infrared radiation followed by a reflecting mirror (to switch the light path from horizontal to vertical) and long-cutoff filters to select for ultraviolet-A (UVA) + visible (Vis) light ($\lambda \geq 324$ nm) or visible light

only ($\lambda \geq 400$ nm) irradiation of reaction solutions. Incident photon flux for UVA light (324 nm $\leq \lambda \leq 400$ nm) and light from the lower end of the visible spectrum (400 nm $\leq \lambda \leq 500$ nm) was measured by potassium ferrioxalate actinometry [44]. During the course of the study, an ignition board and reflecting mirror in the Xe lamp system were replaced, causing a change in incident light intensity. Prior to lamp maintenance, incident photon fluxes were determined to be 9.0×10^{-5} Einstein min^{-1} for UVA light and 1.6×10^{-4} Einstein min^{-1} for visible light. After maintenance, photon fluxes were determined to be 7.2×10^{-5} Einstein min^{-1} for UVA light and 1.1×10^{-4} Einstein min^{-1} for visible light. Throughout the paper, all direct comparisons of rates shown within individual figure plots were conducted either before or after lamp maintenance, and figure captions indicate lamp 1 or lamp 2, respectively, for the two experimental time periods. Experiments examining formation of diatrizoate transformation products under oxic conditions were conducted using a similar lamp setup outfitted with an Oriel O$_3$-free 1000 W xenon arc lamp.

2.3. Photocatalysis experiments

Batch photocatalytic experiments were conducted in 50 mL aqueous TiO$_2$ suspensions that were continuously stirred in 250 mL jacketed glass beakers attached to a circulating constant-temperature water bath maintained at 25 °C. Prior to irradiation, suspensions containing the desired TiO$_2$ loading ($0–1$ g L^{-1}), target ICM concentration (typically 20 μM), and other solution constituents (e.g., methanol, NaHCO$_3$) were prepared and equilibrated in the dark for at least 30 min while sparging with air (for oxic condition) or argon (for anoxic conditions). Sparging gases were first passed through a 1 M NaOH trap to remove traces of CO$_2$ and two water traps to hydrate the gas and minimize evaporation of the TiO$_2$ suspensions during experiments. Suspension pH was continuously controlled using an automatic pH stat device (Radiometer TIM854) equipped with HClO$_4$ or NaOH burettes. After collecting an initial aliquot of suspension (1.5 mL) for $t = 0$, reaction was initiated by placing the pre-equilibrated TiO$_2$ suspension under the lamp and continuing to mix and sparge with gas. Sample aliquots of suspension were then collected from the irradiated reactor at various time steps to monitor reaction progress. Collected aliquots were centrifuged for 30 min (13,200 rpm; Eppendorf centrifuge 5415D) and supernatant was analyzed by high performance liquid chromatography (HPLC) to determine the concentration of target ICM remaining after increasing reaction times.

For experiments examining formation of reaction products under oxic conditions, a series of equivalent 50 mL TiO$_2$ suspensions were prepared at pH 8.0 in the same manner described above and were irradiated for different lengths of time before collecting and filtering (Millipore Millex-HN 0.45 μm) the entire reactor volume for analysis with several analytical techniques. Higher initial concentrations of diatrizoate (200 μM) were also used in product analysis experiments to permit easier analysis of minor reaction products.

2.4. Analytical

Concentrations of diatrizoate and other target ICM were determined by HPLC with UV photodiode array (PDA) detection (Shimadzu AVP System). For diatrizoate and DABA, a Spherisorb ODS-2 C18 column (4.6 mm × 150 mm, 5 μm packing material) and 10 mm guard column of the same material were used for the stationary phase. For diatrizoate, an isocratic mobile phase (1 mL min^{-1}) was used consisting of a 4:96 (v/v) ratio of acetonitrile and an aqueous eluent (20 mM phosphate + 10 mM triethylamine, adjusted to pH 6 with H$_3$PO$_4$). Detector absorbance was monitored at $\lambda = 237$ nm. For DABA, a 2:98 ratio of the same eluents was

used, and absorbance was monitored at $\lambda = 231$ nm. For iopromide, a Novapak C18 column (3.9 mm × 150 mm, 4 μm packing material) and 10 mm guard column of the same material were used as the stationary phase and a gradient method (1 mL min^{-1}) was used consisting of 5 mM ammonium acetate buffer and acetonitrile. The acetonitrile was maintained at 4% (v/v) from 0 to 3 min, then increased linearly to 7.5% from 3 to 10 min, held constant from 10 to 15 min, and finally decreased back to 4% from 15 to 18 min and held constant from 18 to 20 min. Detector absorbance was monitored at $\lambda = 241$ nm. As reported previously [27], doublet peaks are observed for iopromide due to stereoisomerism; quantification was accomplished by integration of both peaks and comparison with reference standards.

Selected organic reaction intermediates and products for diatrizoate reactions were identified using liquid chromatography coupled with tandem mass spectrometry (LC–MS/MS). Analysis was performed using an Agilent 1200 Series LC/MSD Trap XCT Ultra. An Agilent Zorbax SB-C18 column (2.1 mm × 30 mm, 3.5 μm packing material) was used as the stationary phase. An isocratic mobile phase (0.2 mL min^{-1}) was used with a 1:99 (v/v) ratio of two eluents (eluent A: 95% acetonitrile, 5% H$_2$O, and 0.1% formic acid; eluent B: 5 mM acetic acid). Mass spectral analysis was conducted in positive mode electrospray ionization (ESI+) over a mass range of 50–1300 m/z. The fragmentation amplitude used was 1.00 V conducted in auto MS(n) mode optimized for $m/z = 614$.

Changes in total dissolved organic carbon (DOC) concentration were measured using a Shimadzu TOC-VCPH combustion analyzer. Inorganic anions (NO$_3^-$, NO$_2^-$, and I$^-$) were quantified by ion chromatography (Dionex ICS-2000 system equipped with a conductivity detector). The stationary phase was an IonPac AS18 anion-exchange column (4 mm × 200 mm, 7.5 μm packing material), and the mobile phase (1 mL min^{-1}) was 36 mM KOH. Ammonium concentration was determined by colorimetric analysis (Hach method 10023) using a Shimadzu UV-2401PC UV–Vis spectrophotometer.

3. Results and discussion

3.1. Reaction kinetics in oxic systems

Experimental results demonstrate that diatrizoate was photocatalytically degraded in air-saturated (i.e., oxic) aqueous TiO$_2$ suspensions irradiated with UVA light. Fig. 1a shows the results of a representative batch experiment, demonstrating degradation of diatrizoate in UVA-irradiated TiO$_2$ suspensions at circumneutral pH conditions. Greater than 65% of diatrizoate is degraded within 1 h under the conditions shown. In comparison, no significant loss of diatrizoate occurred in TiO$_2$-free solutions irradiated with UVA light or in TiO$_2$ suspensions that were maintained under darkness or irradiated with visible light only ($\lambda > 400$ nm). The lack of significant UVA photolysis observed within 60 min is consistent with previous reports of slow solar direct photolysis of ICM [45]. The requirements of TiO$_2$ + UVA light for achieving significant diatrizoate degradation is consistent with diatrizoate reaction with reactive species generated by semiconductor bandgap photoexcitation [29,30]. Degradation of diatrizoate in UVA-TiO$_2$ batch reactions can be described using a pseudo-first-order kinetic rate law, and the rate constant (k_{obs}) determined for the data in Fig. 1a was $2.1(\pm 0.3) \times 10^{-2}$ min^{-1}. Results from the dark control reaction also demonstrate that diatrizoate adsorption to TiO$_2$ is minimal, with the extent of adsorption being lower than the uncertainty of the HPLC-PDA method (i.e., <5% of added diatrizoate adsorbs) at the conditions examined.

The measured rate constant indicates that diatrizoate is recalcitrant in comparison with other organic pollutants. For example,
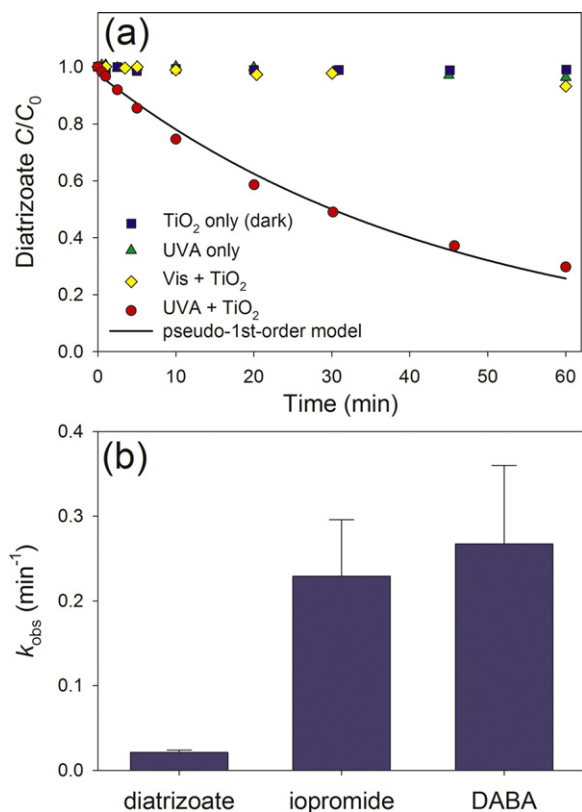
Fig. 1. (a) UVA-TiO$_2$ photocatalytic degradation of diatrizoate in comparison to control experiments in oxic suspensions, and a pseudo-first-order kinetic model fit; (b) comparison of rate constants for photocatalytic degradation of diatrizoate and structural analogues listed in Table 1. Reaction conditions: $C_0 = 20\,\mu$M ICM, 1 g L^{-1} TiO$_2$, pH 8.0, air-sparged, 25 °C, lamp 2. Uncertainties represent triplicate-averaged standard deviations.
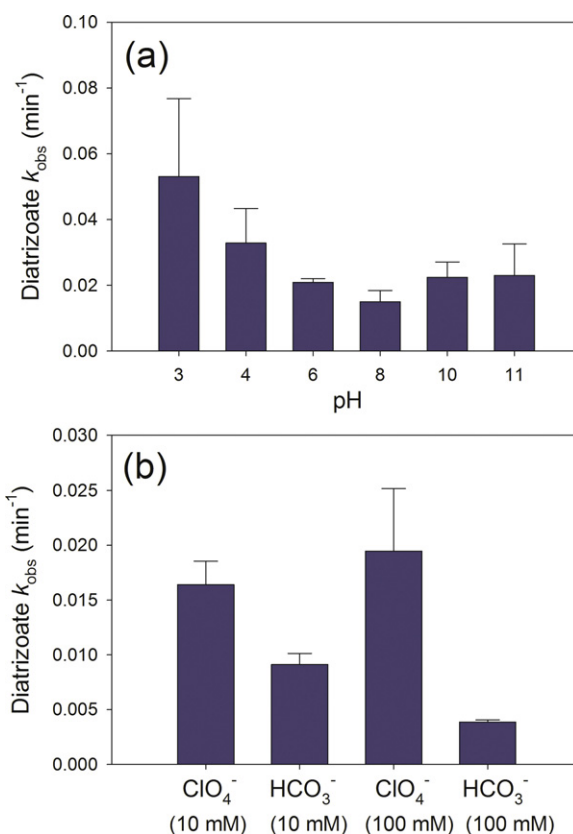

Fig. 2. Effect of (a) pH and (b) dissolved carbonate on rate constants for photocatalytic degradation of diatrizoate. Reaction conditions: $C_0 = 20\,\mu$M diatrizoate, 25 °C, air-sparged, pH 3–11 and 0.25 g L^{-1} TiO$_2$ under lamp 1 (panel a), pH 8.0, NaHCO$_3$ (10, 100 mM), and 1 g L^{-1} TiO$_2$ under lamp 2 (panel b). Uncertainties represent triplicate-averaged standard deviations.

the rate constant for diatrizoate is nearly 10-fold lower than that measured for the sulfonamide antibiotic sulfamethoxazole using the same experimental setup and similar solutions conditions ($k_{obs} = 2.0 \times 10^{-1}$ min^{-1} for $C_0 = 21\,\mu$M, 100 mg L^{-1} TiO$_2$, pH 9). This finding is consistent with previous reports on the high recalcitrance of ICM in general, and diatrizoate in particular, during advanced oxidation processes [9,12,25].

The high recalcitrance of ICM relative to other organic micropollutants can be attributed, in part, to the stabilizing effect of the 2,4,6-triiodinated substituents on the central aromatic ring. This is supported by the much faster rate of photocatalytic oxidation that was observed for DABA, a structural analogue to diatrizoate that lacks the three iodine substituents on the central aromatic ring (Fig. 1b). The measured k_{obs} value for DABA (2.7×10^{-1} min^{-1}) is more than an order-of-magnitude greater than that measured for diatrizoate under the same conditions.

The recalcitrance of diatrizoate can also be attributed partly to the ionic charge of the ICM. Results presented in Fig. 1b also show that the rate constant for photocatalytic degradation of iopromide, a nonionic ICM, is also more than an order-of-magnitude larger than that measured for the anionic diatrizoate. The difference in rates may be due, in part, to the weaker adsorption to TiO$_2$ expected for diatrizoate than iopromide. Although quantitatively both compounds adsorb weakly to TiO$_2$ (i.e., <5% of added ICM adsorbs) and it is difficult to accurately measure the extent of adsorption, reactant adsorption is still believed to be critical to surface-catalyzed processes [29,46]. It follows that it is reasonable to expect that electrostatic repulsion of the anionic diatrizoate (p$K_a = 3.4$ [47]) by the negatively charged TiO$_2$ surface at pH 8 (pH$_{zpc}$ 6.25 [29]) will

lead to a lower extent of adsorption in comparison to the nonionic iopromide.

The influence of diatrizoate adsorption on photocatalysis kinetics can also be used to explain the observed effect of pH. Fig. 2a shows that observed rate constants are roughly constant at pH $\geq$ 6, but increase by nearly a factor of three when suspensions are acidified to pH 3. Although the extent of diatrizoate adsorption was small under all pH conditions examined and could not be measured accurately using procedures employed in this study, the observed pH-dependent trend in k_{obs} is consistent with well documented pH-dependent trends in the extent to which benzoic acid and analogues adsorb to variably-charged metal oxide surfaces similar to TiO$_2$ [48,49]. In addition, changes in pH can also affect other processes like nanoparticle aggregation, which can also affect rates of photocatalytic processes.

3.2. Identification of photo-generated reactive species

To identify the important photo-generated reactive species for diatrizoate transformation in the presence of TiO$_2$, reaction rates were measured in batch reactors where solutions were modified by introducing known radical scavengers and electron acceptors (Fig. 3). First, adding a large excess concentration of methanol (1 M), a hydroxyl radical scavenger [50], to an air-sparged suspension markedly inhibited the photocatalytic degradation of diatrizoate, decreasing k_{obs} by 80%. Such marked inhibition of the reaction implies that under oxic conditions, diatrizoate degradation occurred principally through oxidation by adsorbed $^\bullet$OH (surface trapped valence band holes) [51]. This finding is consistent with the dominant oxidative photocatalytic pathway identified for a
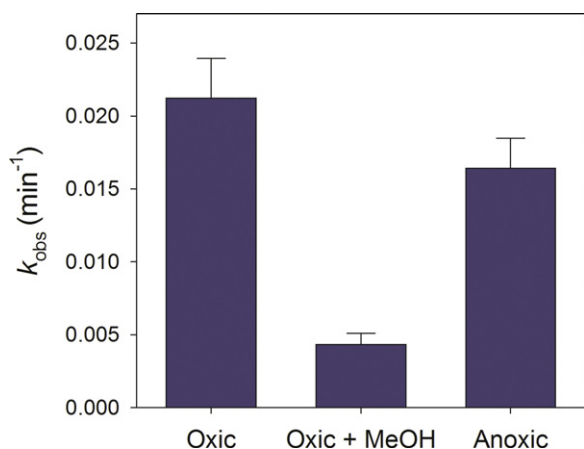
Fig. 3. Effects of adding methanol and removing dissolved O_2 on rate constants for photocatalytic degradation of diatrizoate. Reaction conditions: $C_0 = 20\,\mu M$ diatrizoate, $1\,g\,L^{-1}$ TiO_2, pH 8.0, 25 °C, lamp 2, 1 M methanol, air-sparging (oxic conditions) or argon-sparging (anoxic conditions). Uncertainties represent triplicate-averaged standard deviations.

diverse range of organic contaminants [7,10,32,36,43]. The predominance of ICM reactions with adsorbed •OH is also supported by the relative reactivity trends already noted for diatrizoate, DABA, and iopromide (Fig. 1b). Jeong et al. [52] reported that diatrizoate was significantly less reactive with •OH generated in homogeneous solution (by pulse radiolysis) than DABA and iopromide. However, the relative difference in homogeneous •OH rate constants between diatrizoate and the two structural analogues (diatrizoate: $k_2 = 9.58 \times 10^8\,M^{-1}\,s^{-1}$; DABA: $k_2 = 6.0 \times 10^9$; iopromide: $k_2 = 3.34 \times 10^9$) was still smaller than the difference in apparent photocatalytic rate constants shown in Fig. 1b, likely due to additional variations in adsorptive interactions with the TiO_2 surface (i.e., variations in the adsorption parameter within a Langmuir–Hinshelwood kinetic model for surface reactions [46]) that are not relevant reactions with solution phase •OH.

According to Scheme 1, the availability of photo-generated •OH for oxidation of organic contaminants also requires an appropriate electron acceptor to react with e_{cb}^- and prevent its buildup and increased rate of recombination with h_{vb}^+ (*pathways r1* with *o1*) [29]. Under oxic conditions, O_2 can adsorb to the TiO_2 surface and react with e_{cb}^- [29], so oxidation of diatrizoate by adsorbed

•OH is coupled with O_2 reduction (i.e., coupling of *pathways o2* with *r2*). Thus, it might be expected that removal of dissolved O_2 would inhibit the photocatalytic degradation of diatrizoate. Instead, results presented in Fig. 3 show that k_{obs} only decreased slightly when the TiO_2 suspension were made anoxic by sparging with an inert gas (argon) in place of air (k_{obs} only dropped from 2.1×10^{-2} to $1.6 \times 10^{-2}\,min^{-1}$). In comparison, photocatalytic degradation of the antibiotics sulfamethoxazole and ciprofloxacin was completely inhibited by removal of dissolved oxygen in similar experiments [7,10]. A plausible explanation for these observations is that diatrizoate, itself, can also act as a conduction band electron acceptor [34,53] in the absence of the more favorable O_2 (i.e., *replace pathway r2 with r3*). This would prevent buildup of e_{cb}^- and consequential shutdown of photocatalysis by increased charge carrier recombination (combination of *pathways r1 + o1*). Thus, in anoxic solutions, diatrizoate can react with both •OH and e_{cb}^- under anoxic conditions (i.e., coupling of *pathways o2* with *r3*).

Although, to our knowledge, there are no previous reports of photocatalytic reduction of diatrizoate or related ICM, previous literature reports support the favorability of photocatalytic reduction processes for ICM. First, the UV-TiO_2 photocatalytic reductive dehalogenation of chlorinated organic compounds has been documented [34,53], and reductive deiodination and debromination processes are generally more rapid than dechlorination processes [35,37]. In addition, recent studies report reductive deiodination of ICM by Pd-based catalysts and zerovalent iron [26–28], and Jeong et al. [52] showed that strongly reducing hydrated electrons (e_{aq}^-) were much more reactive with ICM than with lesser iodinated and deiodinated structural analogues.

The observation that excess methanol addition to oxic TiO_2 suspensions did not completely inhibit photocatalytic degradation suggests that reductive dehalogenation of diatrizoate by e_{cb}^- may also be a minor contributor to diatrizoate transformation under oxic treatment condition. However, additional research is needed to identify the specific mechanism(s) responsible for the residual level of treatment observed in methanol-amended oxic TiO_2 suspensions because methanol scavenging of •OH can produce a α-hydroxymethyl radical (•CH_2OH), which is a strong one-electron reductant itself [54].

3.3. Effects of dissolved carbonate

Bicarbonate, a common ionic constituent of natural waters, inhibited the photocatalytic degradation of diatrizoate (Fig. 2b). Addition of 10 mM and 100 mM $NaHCO_3$ lowered the observed rate constants by 45% and 80%, respectively, relative to control reactions conducted in an inert electrolyte ($NaClO_4$) of equivalent ionic strength. These results are consistent with previous reports that dissolved carbonate species act as •OH scavengers in natural waters [55,56]:

$$HCO_3^- + {}^\bullet OH \rightarrow CO_3^{\bullet -} + H_2O \tag{1}$$

$$CO_3^{2-} + {}^\bullet OH \rightarrow CO_3^{\bullet -} + OH^- \tag{2}$$

The resulting carbonate radical is a weaker oxidizing agent that is expected to react minimally with most organic contaminants [56,57]. In terms of the pathways depicted in Scheme 1, dissolved carbonate species are then inhibiting oxidation of diatrizoate by the same mechanism as methanol (i.e., *pathway o3* outcompeting *pathway o2 for adsorbed •OH*). Some of the observed inhibition may also be due to competitive inhibition of diatrizoate adsorption by adsorption of the dissolved carbonate species. Results demonstrate a significant inhibitory effect of dissolved carbonate species, which will be critical to the design of practical treatment systems. Thus, future work examining these effects in greater detail in combination with other water quality variables (e.g., pH, hardness) will
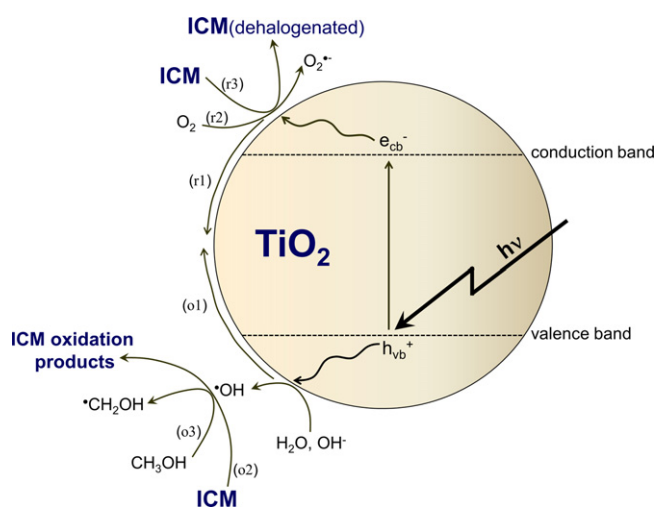
Scheme 1. Major reaction pathways controlling UV-TiO_2 photocatalytic degradation of diatrizoate under oxic and anoxic conditions. Letters in parentheses indicate reaction pathways for the photo-generated oxidant (o1–o3) and reductant (r1–r3) discussed in the text.
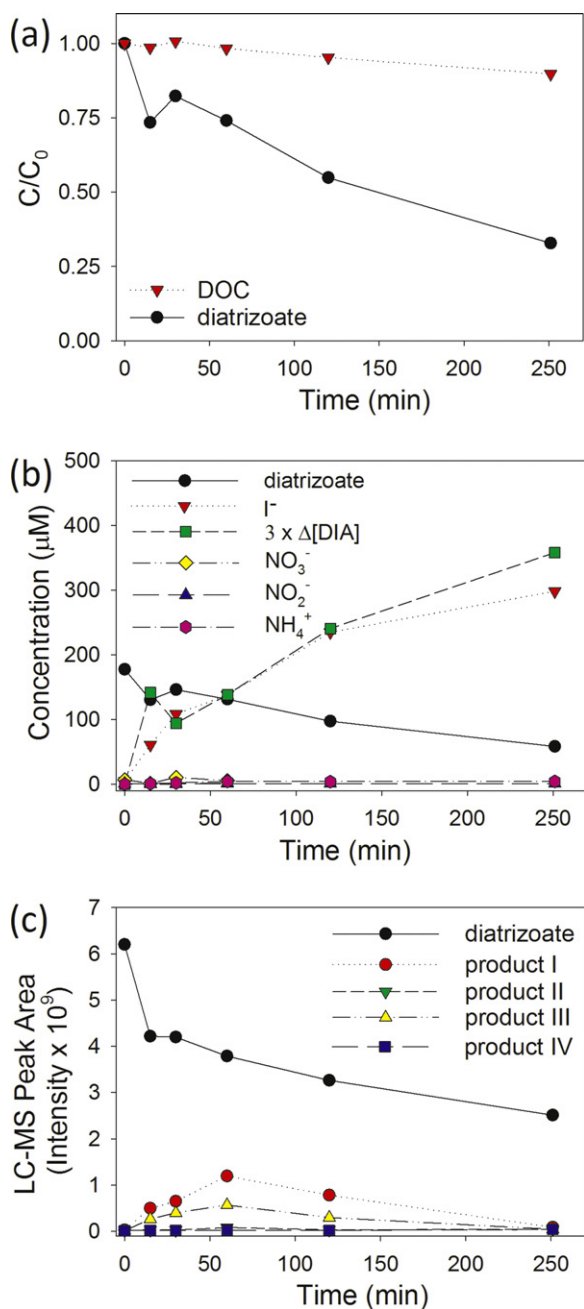
Fig. 4. Summary of products formed by UVA-TiO$_2$ photocatalytic degradation of diatrizoate under oxic conditions. (a) Comparison of diatrizoate degradation with changes in DOC, (b) formation of inorganic ions in comparison to diatrizoate degradation, and (c) changes in LC–MS TIC peak areas for diatrizoate and organic transformation products listed in Table 2. Reaction Conditions: $C_0 = 200\,\mu$M diatrizoate, 1 g L^{-1} TiO$_2$, pH 8.0, 25 °C, air sparged, 1000 W Xe lamp.

be needed to develop predictive treatment models applicable to diverse sourcewaters.

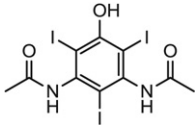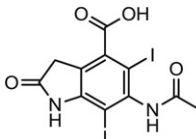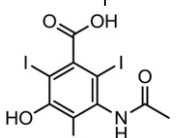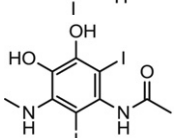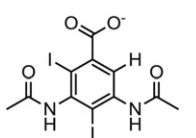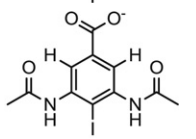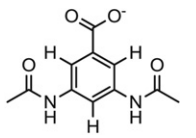### 3.4. Photocatalysis reaction products and pathways
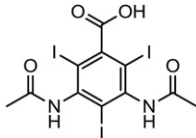
A detailed analysis of reaction products was performed for oxidative UVA-TiO$_2$ photocatalysis of diatrizoate (Fig. 4) since this is the process that is likely to predominate when treating aerated source waters (e.g., surface drinking water sources, polishing treatment at water reclamation facilities). Fig. 4a shows that little change in DOC occurred during the initial stages of photocatalytic oxidation of diatrizoate. Whereas 67% of the 200 μM initial

diatrizoate concentration was transformed during the time monitored, DOC decreased by only ∼10%. Thus, initial reactions with •OH do not leading to significant mineralization, but instead to formation of other organic products. Similar findings have been previously reported in studies on ICM treatment by photocatalytic [40] and O$_3$/H$_2$O$_2$ [58] processes. In addition, only minimal production of inorganic nitrogen species (NH$_4^+$, NO$_3^-$, and NO$_2^-$) was observed (Fig. 4b), which implies much of the nitrogen remained bound to the organic transformation products.

In contrast to carbon and nitrogen measurements, iodide measurements indicate that the 3 iodine substituents bonded to the central aromatic ring were liberated almost stoichiometrically without significant lag upon diatrizoate oxidation. This is illustrated by comparing the measured production of I$^-$ with the theoretical maximum concentration produced if complete dehalogenation occurred coincident with oxidative transformation of the parent compound at each timepoint (i.e., $3 \times \Delta$[diatrizoate]). This finding is somewhat surprising given the lack of carbon and nitrogen mineralization. However, complete liberation of iodine while maintaining DOC was also reported for diatrizoate oxidation by O$_3$/H$_2$O$_2$ treatment (which also generates •OH) [58]. Doll and Frimmel [40] reported a lower extent of iodine liberation (∼60%) with some initial lag time during the UVA-TiO$_2$ treatment of iomeprol, a nonionic ICM. However, only ∼40% of iodine was liberated for iomeprol during O$_3$/H$_2$O$_2$ treatment compared to ∼100% for diatrizoate [58], indicating that the latter ICM is more susceptible to iodine release than iomeprol. Jeong et al. [52] reported only ∼30% iodide release from diatrizoate in γ-irradiated solutions where reactions of •OH is the predominant oxidant species present, suggesting that other reactive species must contribute to iodide release during UVA-TiO$_2$ and O$_3$/H$_2$O$_2$ treatment.

Together, the observed trends in DOC and inorganic products suggest that diatrizoate was being transformed predominantly to organic products wherein the nitrogen atoms are retained, but the iodine substituents are liberated. LC–MS/MS analysis was conducted to identify organic intermediates and products resulting from photocatalytic oxidation of diatrizoate, but these analyses only revealed four organic products whose proposed tentative structures are summarized in Table 2 (Products I–IV); mass fragmentation data and extracted ion chromatograms are provided as Supplementary Material. Three of the four proposed products retain both of the nitrogen atoms from the parent compound (1 of the two N cleaved in the fourth product), and very few carbon atoms are removed, consistent with the inorganic nitrogen and DOC measurements. However, the proposed structures are inconsistent with the expected major organic transformation products because two of the four products retain all three iodine substituents and the other two products retain two iodine substituents. Thus, these compounds likely represent only minor products and the major oxidation products are not amenable to the LC–MS/MS analysis method used here. This conclusion is semi-quantitatively supported by LC–MS total ion chromatogram (TIC) data. Although reference standards are not available for these compounds and differences in ionization efficiency do not allow for direct quantification, the observed TIC peak areas for the four products were small in comparison with the decrease in the TIC peak area observed for diatrizoate during the reaction (Fig. 4c). Thus, if differences in ionization were not so large, it can be concluded that the identified products represented only a minor fraction of those actually formed by photocatalytic oxidation of diatrizoate. Nonetheless, because iodide release is near stoichiometric during the process, the major organic intermediates most likely were dehalogenated [52]. Mechanisms for oxidative dehalogenation of aromatic compounds have been previously reported for aqueous and adsorbed •OH, initiated by oxidant attack at the halide ring positions followed by rapid reactions that lead to elimination of the halide substituent [29,52].

Table 2
Reaction products and intermediates identified by LC–MS/MS analysis.

Product ID	[M + H]+ (m/z)[a]	MS/MS (m/z)	Difference with DIA	Proposed structure
DIA	615	488, 361, 233		(structure)
Oxic conditions – oxidative transformation[c]				
I	587	460, 333, 205	-COOH +OH	(structure)
II	487	469, 360, 359, 341, 318, 300, 233	-I -H	(structure)
III	574	447, 320	-C$_2$H$_4$NO +OH	(structure)
IV	449	431, 403, 320, 304, 276	-I -COOH -CO +2OH	(structure)
Anoxic conditions – reductive transformation[c]				
V[b]	489	235	-I +H	(structure)
VI[b]	363	345, 236, 194, 152	-2I +2H	(structure)
VII (DABA)	237	219	-3I +3H	(structure)

[a] Mass of pseudomolecular ion formed by protonation of the neutral molecule shown in the structure.

[b] The positions of remaining iodine substituents could not be determined from LC–MS data, so structure shown is accurate with respect to the number of iodine substituents remaining, but not necessarily the positioning on the aromatic ring structure.

[c] Oxic conditions = air-sparged suspensions. Anoxic conditions = argon-sparged suspensions amended with methanol to supress reaction of diatrizoate with •OH.

The rapid release of all three iodine substituents coincident with diatrizoate loss suggests that some other reactive species generated in the UVA-TiO$_2$ photocatalytic system (e.g., O$_2$•−, e$_{cb}$−) is reacting rapidly with organic reaction intermediates to promote complete dehalogenation. Additional research using complementary mass spectrometry and spectroscopic methods (e.g., NMR) is needed to further elucidate the responsible mechanisms.

The four minor products that were identified can be formed by a variety of mechanisms. The most abundant of these in terms of LC–MS TIC data (Fig. 4c), product IV, can form by commonly reported photo-Kolbe decarboxylation reactions involving electron transfer [59]. Jeong et al. [52] also reported product IV as the major •OH oxidation product for diatrizoate detected in homogeneous aqueous solution and proposed an electrophilic aromatic substitution mechanism wherein •OH attacks at the carboxylate position

followed by release of carbonate radical. The other products can form by reactions initiated at the amide side chains. The cyclic product II can form by H atom abstraction from the terminal methyl group [29] followed by intramolecular attack of the resulting carbon radical at the neighboring iodo position. Product III can form by •OH attack on the aromatic ring at one of the amide positions and elimination of the amide side chain. Product IV contains multiple structural changes consistent with oxidation of the amide side chains [60] together with oxidative dehalogenation and decarboxylation processes already described.

Results presented in Fig. 3 demonstrate that diatrizoate may also be subject to reduction by photo-generated e$_{cb}$−, particularly in anoxic solutions. LC–MS/MS analysis indicated formation of 3 products in anoxic suspensions which differed from the parent compound mass only in the number of iodine substituents
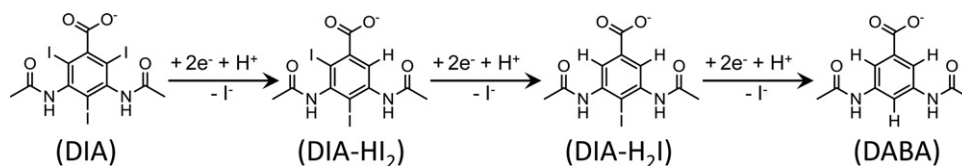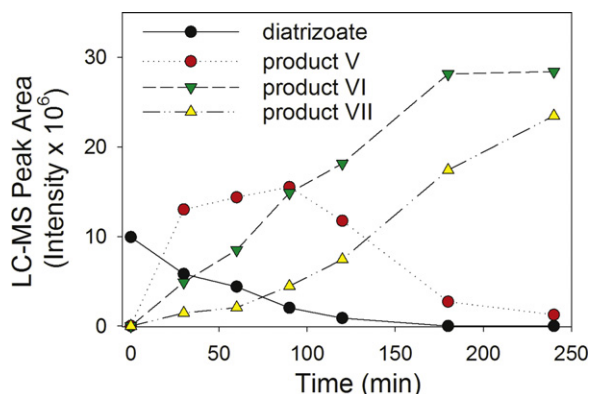
Scheme 2. Reductive deiodination of diatrizoate.

Fig. 5. Time-dependent changes in LC–MS TIC chromatogram peak areas for diatrizoate and organic transformation products observed under anoxic reductive treatment conditions described in Fig. 3.

(tentative structures summarized in Table 2, Products V–VII; mass fragmentation data and extracted product ion chromatograms provided as Supplementary Material). Time dependent changes in the extracted ion chromatograms of the three products (Fig. 5) are consistent with diatrizoate transformation via sequential reductive deiodination (Scheme 2) in the absence of O_2, similar to reactions reported for other strong reducing agents (e.g., Pd-H_{ads}, Fe(0)) [26–28,52]. This finding also follows from previous reports on photocatalytic reductive dehalogenation of chlorinated organic compounds by e_{cb}^- [34,53].

4. Conclusions

Results from this study demonstrate that UV-TiO_2 photocatalysis can be an effective technology for transforming diatrizoate in both oxic and anoxic aquatic systems. Experiments demonstrate that diatrizoate degradation under oxic conditions relies on reactions with adsorbed hydroxyl radicals generated in accordance with the semiconductor charge separation mechanism. A variety of organic and inorganic products are detected, consistent with the non-selective reactivity of •OH at different sites within the diatrizoate structure. At short reaction times, photocatalytic oxidation yields minimal mineralization of organic C and N in the parent molecule, but stoichiometric iodide is released. Under anoxic conditions, appreciable rates of diatrizoate photocatalytic degradation are observed, and products identified by LC–MS/MS analysis indicate predominance of reductive deiodination pathways. Release of iodide by both oxidative and reductive pathways is significant, because the resulting deiodinated products are expected to be much more biodegradable in downstream processes and in receiving waters. Discovery of the reductive transformation pathway for diatrizoate is also potentially useful for developing more selective treatment technologies for ICM. Whereas the oxidative pathway, which relies on the non-selective •OH to transform diatrizoate, is likely to be severely inhibited in wastewater and drinking water because of radical scavenging by natural organic matter and dissolved carbonate species, reductive processes are inherently more chemical selective and should be less prone to competitive

inhibition by natural water constituents. Further research is suggested to examine development of practical photocatalytic reduction processes for ICM.

Appendix A. Supplementary data

Supplementary data associated with this article can be found, in the online version, at http://dx.doi.org/10.1016/j.apcatb.2012.09.013.

References

[1] C.G. Daughton, T.A. Ternes, Environmental Health Perspectives 107 (1999) 907.
[2] B. Halling-Sørensen, S. Nors Nielsen, P.F. Lanzky, F. Ingerslev, H.C. Holten Lützhøft, S.E. Jørgensen, Chemosphere 36 (1998) 357–393.
[3] T. Heberer, Toxicology Letters 131 (2002) 5–17.
[4] R. Hirsch, T. Ternes, K. Haberer, K.-L. Kratz, Science of the Total Environment 225 (1999) 109–118.
[5] D.W. Kolpin, E.T. Furlong, M.T. Meyer, E.M. Thurman, S.D. Zaugg, L.B. Barber, H.T. Buxton, Environmental Science and Technology 36 (2002) 1202–1211.
[6] M.C. Dodd, C.-H. Huang, Environmental Science and Technology 38 (2004) 5607–5615.
[7] L. Hu, P.M. Flanders, P.L. Miller, T.J. Strathmann, Water Research 41 (2007) 2612–2626.
[8] L. Hu, H.M. Martin, O. Arce-Bulted, M.N. Sugihara, K.A. Keating, T.J. Strathmann, Environmental Science and Technology 43 (2008) 509–515.
[9] M.M. Huber, S. Canonica, G.-Y. Park, U. von Gunten, Environmental Science and Technology 37 (2003) 1016–1024.
[10] T. Paul, P.L. Miller, T.J. Strathmann, Environmental Science and Technology 41 (2007) 4720–4727.
[11] J.E. Drewes, P. Fox, M. Jekel, Journal of Environmental Science and Health, Part A: Toxic/Hazardous Substances & Environmental Engineering 36 (2001) 1633–1645.
[12] W. Seitz, J. Jiang, W.H. Weber, B.J. Lloyd, M. Maier, D. Maier, Environmental Chemistry 3 (2006) 35–39.
[13] T.A. Ternes, R. Hirsch, Environmental Science and Technology 34 (2000) 2741–2748.
[14] R.L. Oulton, T. Kohn, D.M. Cwiertny, Journal of Environmental Monitoring 12 (2010) 1956–1978.
[15] M. Jekel, T. Reemtsma, Organic Pollutants in the Water Cycle: Properties, Occurence, Analysis, and Environmental Relevance of Polar Compounds, Wiley-VCH, Weinheim, 2006.
[16] S. Pérez, D. Barceló, Analytical and Bioanalytical Chemistry 387 (2007) 1235–1246.
[17] A. Putschew, S. Wischnack, M. Jekel, Science of the Total Environment 255 (2000) 129–134.
[18] M. Schulz, D. Loffler, M. Wagner, T.A. Ternes, Environmental Science and Technology 42 (2008) 7207–7217.
[19] D. Weissbrodt, L. Kovalova, C. Ort, V. Pazhepurackel, R. Moser, J. Hollender, H. Siegrist, C.S. McArdell, Environmental Science and Technology 43 (2009) 4810–4817.
[20] M.E. Gale, A.H. Robbins, R.J. Hamburger, W.C. Widrich, American Journal of Roentgenology 142 (1984) 333–335.
[21] H.D. Humes, D.A. Hunt, M.D. White, American Journal of Physiology 252 (1987) F246–F255.
[22] A.L. Batt, S. Kim, D.S. Aga, Environmental Science and Technology 40 (2006) 7367–7373.
[23] J.L. Kormos, M. Schulz, H.P.E. Kohler, T.A. Ternes, Environmental Science and Technology 44 (2010) 4998–5007.
[24] P. Westerhoff, Y. Yoon, S. Snyder, E. Wert, Environmental Science and Technology 39 (2005) 6649–6663.

[25] T.A. Ternes, J. Stüber, N. Herrmann, D. McDowell, A. Ried, M. Kampmann, B. Teiser, Water Research 37 (2003) 1976–1982.

[26] T. Hennebel, S. De Corte, L. Vanhaecke, K. Vanherck, I. Forrez, B. De Gusseme, P. Verhagen, K. Verbeken, B. Van der Bruggen, I. Vankelecom, N. Boon, W. Verstraete, Water Research 44 (2010) 1498–1506.

[27] L.E. Knitt, J.R. Shapley, T.J. Strathmann, Environmental Science and Technology 42 (2007) 577–583.

[28] M. Stieber, A. Putschew, M. Jekel, Water Science and Technology 57 (2008) 1969–1975.

[29] M.R. Hoffmann, S.T. Martin, W. Choi, D.W. Bahnemann, Chemical Reviews 95 (1995) 69–96.

[30] A.G. Agrios, K.A. Gray, E. Weitz, Langmuir 19 (2003) 1402–1409.

[31] L. Cermenati, A. Albini, P. Pichat, C. Guillard, Research on Chemical Intermediates 26 (2000) 221–234.

[32] I.K. Konstantinou, T.A. Albanis, Applied Catalysis B: Environmental 42 (2003) 319–335.

[33] T. Pandiyan, O. Martínez Rivas, J. Orozco Martínez, G. Burillo Amezcua, M.A. Martínez-Carrillo, Journal of Photochemistry and Photobiology A: Chemistry 146 (2002) 149–155.

[34] W.H. Glaze, J.F. Kenneke, J.L. Ferry, Environmental Science and Technology 27 (1993) 177–184.

[35] W. Choi, M.R. Hoffmann, Journal of Physical Chemistry 100 (1996) 2161–2169.

[36] G.K.C. Low, S.R. McEvoy, R.W. Matthews, Environmental Science and Technology 25 (1991) 460–467.

[37] W. Choi, M.R. Hoffmann, Environmental Science and Technology 31 (1997) 89–95.

[38] A. Haiß, K. Kümmerer, Chemosphere 62 (2006) 294–302.

[39] W. Kalsch, Science of the Total Environment 225 (1999) 143–153.

[40] T.E. Doll, F.H. Frimmel, Water Research 38 (2004) 955–964.

[41] T.E. Doll, F.H. Frimmel, Catalysis Today 101 (2005) 195–202.

[42] T.E. Doll, F.H. Frimmel, Water Research 39 (2005) 403–411.

[43] J. Theurich, M. Lindner, D.W. Bahnemann, Langmuir 12 (1996) 6368–6376.

[44] C.G. Hatchard, C.A. Parker, Proceedings of the Royal Society (London) A235 (1956) 518–536.

[45] T.E. Doll, F.H. Frimmel, Chemosphere 52 (2003) 1757–1769.

[46] M.A. Vannice, Kinetics of Catalytic Reactions, Springer, New York, 2005.

[47] H.H. Lerner, Analytical Profiles of Drug Substances, Academic Press, New York, 1975.

[48] S. Chou, C. Huang, Chemosphere 38 (1999) 2719–2731.

[49] R. Kummert, W. Stumm, Journal of Colloid and Interface Science 75 (1980) 373–385.

[50] C. Galindo, P. Jacques, A. Kalt, Journal of Photochemistry and Photobiology A: Chemistry 130 (2000) 35–47.

[51] H. Lee, W. Choi, Environmental Science and Technology 36 (2002) 3872–3878.

[52] J. Jeong, J. Jung, W.J. Cooper, W. Song, Water Research 44 (2010) 4391–4398.

[53] L.L. Lifongo, D.J. Bowden, P. Brimblecombe, Chemosphere 55 (2004) 467–476.

[54] W. Choi, M.R. Hoffmann, Environmental Science and Technology 29 (1995) 1646–1654.

[55] D.S. Bhatkhande, V.G. Pangarkar, A.A.C.M. Beenackers, Journal of Chemical Technology and Biotechnology 77 (2002) 102–116.

[56] S. Canonica, T. Kohn, M. Mac, F.J. Real, J. Wirz, U. Von Gunten, Environmental Science and Technology 39 (2005) 9182–9188.

[57] J. Huang, S.A. Mabury, Environmental Toxicology and Chemistry 19 (2000) 1501–1507.

[58] B. Ning, N.J.D. Graham, Journal of Environmental Engineering 134 (2008) 944–953.

[59] Y. Mao, C. Schoneich, K.-D. Asmus, Journal of Physical Chemistry 95 (1991) 10080–10089.

[60] H.M.K.K. Pathirana, R.A. Maithreepala, Journal of Photochemistry and Photobiology A: Chemistry 102 (1997) 273–277.